Compact Modeling of pH-Sensitive FETs Based on 2-D Semiconductors

Tarek El Grour, Francisco Pasadas, Alberto Medina-Rull, Montassar Najari, Enrique G. Marin, Alejandro Toral-Lopez, Francisco G. Ruiz, Andrés Godoy, David Jiménez, and Lassaad El Mir

Abstract— We present a physics-based circuit-compatible model for pH-sensitive field-effect transistors based on 2-D materials. The electrostatics along the electrolyte-gated 2-D-semiconductor stack is treated by solving the Poisson equation, including the site-binding model and the Gouy–Chapman–Stern approach, while the carrier transport is described by the drift-diffusion theory. The proposed model is provided in an analytical form and then implemented in Verilog-A, making it compatible with standard technology computer-aided design tools employed for circuit simulation. The model is benchmarked against two experimental transition-metal-dichalcogenide (MoS_2 and ReS_2)-based ion sensors, showing excellent agreement when predicting the drain current, threshold voltage shift, and current/voltage sensitivity measurements for different pH concentrations.

Index Terms— 2-D material, electrolyte, field-effect transistor (FET), ion-sensitive FET (ISFET), pH sensor, transition metal dichalcogenide (TMD), Verilog-A.

I. Introduction

THE 2-D semiconductors combine excellent electrostatics and electronic transport properties with high surface-to-volume ratio, ultimate scaling limits, flexibility, and the feasibility to large-scale processing and manufacturing, constituting great candidates for low-cost wearable and implantable biosensors [1], [2]. In this regard, field-effect transistors (FETs) based on transition metal dichalcogenides (TMDs) are receiving considerable attention due to their ability to perform label-free electrical detection of biological species, such as proteins, DNA, and several biomolecules [3]–[7]. Their use as ion-sensitive FETs (ISFETs) has also been widely demonstrated showing excellent detection capabilities and, in the particular case of pH, high stability, and near-ideal pH voltage sensitivity, close to the Nernst limit (around 59 mV/pH at room temperature) [4], [5], [8]–[10]. This state of the art at the device level foresees their soon application in advanced bioelectronics circuits. It is in this forthcoming arena where 2-D-ISFETs compact modeling becomes extremely useful, not only to interpret electrical measurements or predict the device and circuit optimal operation but also to assist and expedite the design of novel prototypes able to leverage the unique properties of TMDs, as well as to benchmark them against conventional technologies.

The work presented in this brief develops a comprehensive description of the 2-D-ISFET operation by combining a verified compact model of 2-D-semiconductor FETs (2DFETs) [11] with the modeling of the solid–liquid interface through the site-binding model and the Gouy–Chapman–Stern approach [12]. The compact model here proposed constitutes the first description of 2-D-ISFETs for pH sensing that is compatible with standard technology computer-aided design (TCAD) tools employed for circuit simulation. In the following, we present the theory behind the electrostatics and carrier transport (Section II), and we validate the predictive capabilities of the model with measurements of two experimental TMD (MoS_2 and ReS_2)-based ISFETs for pH sensing (Section III). Finally, the main conclusions are drawn in Section IV.

II. Drain Current Modeling of 2-D-ISFETs

Fig. 1(a) shows a schematic depiction of a 2-D-ISFET, whose structure consists of a FET where the top-gate metal is substituted by an electrolyte solution with a reference electrode immersed in it. In addition to the induced charge in the electrolyte, the electrostatic modulation of the carrier concentration in the 2-D sheet is achieved via the reference electrode (V_g) and a bottom gate contact (V_b) coupled through a bottom
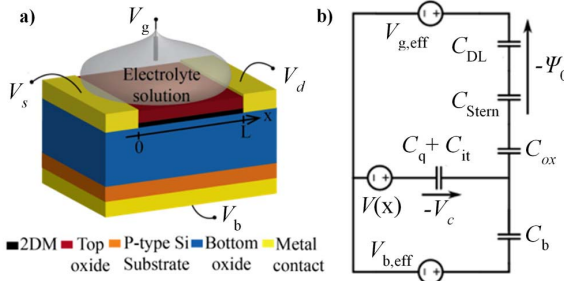
Fig. 1. (a) Schematic depiction of a 2-D-ISFET. (b) Equivalent capacitive circuit of the 2-D-ISFET.

dielectric. The top oxide acts as a barrier, guaranteeing an unambiguous field-effect transduction mechanism through the electrostatic control of the channel. The 1-D electrostatics along a vertical cut of the 2-D-ISFET can be described using the equivalent capacitive circuit, shown in Fig. 1(b), that sets the following charge-balance equation:

$$Q_{\text{net}}(x) + Q_{\text{it}}(x) = -C_{\text{ox}}(V_{\text{g,eff}} + \Psi_0 - V(x) + V_c(x)) \\ - C_{\text{b}}(V_{\text{b,eff}} - V(x) + V_c(x)) \quad (1)$$

where Q_{net} represents the overall net mobile sheet charge density at the 2-D channel and $C_{\text{ox}} = \varepsilon_{\text{ox}}/t_{\text{ox}}$ ($C_{\text{b}} = \varepsilon_{\text{b}}/t_{\text{b}}$) is the top (bottom) oxide capacitance, with ε_{ox} (ε_{b}) the top (bottom) dielectric constant and t_{ox} (t_{b}) the top (bottom) oxide thickness. The top (bottom) overdrive voltage is $V_{\text{g,eff}} = V_{\text{g}} - V_{\text{g0}}$ ($V_{\text{b,eff}} = V_{\text{b}} - V_{\text{b0}}$), where V_{g} (V_{b}) is the reference electrode (bottom gate) potential and V_{g0} (V_{b0}) comprises the work-function difference between the electrode (bottom gate) and the 2-D channel as well as additional fixed charge due to impurities or doping [13]. Finally, Ψ_0 is the potential drop at the electrolyte–oxide interface (i.e., the surface potential).

The ISFET operation is grounded on the interaction between the surface charge density (N_s) [14] generated by the chemical reactions taking place at the top oxide–electrolyte interface and the free charge carriers present in the semiconductor. This interaction, and specifically the adsorption of H^+ ions, is governed by the site-binding model [14], whose standard formulation [12] is adopted here. The pH variations of the electrolyte solution are related to Ψ_0 as

$$\Psi_0 = \ln[10](\text{pH}_{\text{pzc}} - \text{pH})\frac{\beta}{1 + \beta}V_{\text{th}} \\ \text{pH}_{\text{pzc}} = \frac{\text{pK}_a + \text{pK}_b}{2} \quad (2)$$

where $V_{\text{th}} = k_{\text{B}}T/q$ is the thermal voltage, k_{B} is Boltzmann's constant, T is the temperature, and q is the elementary charge. pH_{pzc} is the pH value at the charge neutrality point of the oxide surface, β is defined by the Gouy–Chapman–Stern model, and pK_a and pK_b correspond to the dissociation constants. At the electrolyte–insulator interface, the Gouy–Chapman approach describes the double layer as a function of the ionic strength in terms of the capacitance C_{DL}. However, this model overestimates the interface charge [12]. To correct this effect, a region depleted of ionic charges close to the surface is included, giving rise to the so-called Stern capacitance, C_{Stern} [15]. Thus

$$\beta = q N_s \frac{\delta}{C_{\text{eq}} V_{\text{th}}}; \quad \delta = 2 \cdot 10^{\frac{\text{pK}_a - \text{pK}_b}{2}}; \quad C_{\text{eq}} = \frac{C_{\text{DL}} C_{\text{Stern}}}{C_{\text{DL}} + C_{\text{Stern}}} \quad (3)$$

where C_{DL} [12] can be computed as follows:

$$C_{\text{DL}} = \frac{\sqrt{8\varepsilon_{\text{W}} V_{\text{th}} q n_0}}{2 V_{\text{th}}}; \quad n_0 = N_A i_0 \quad (4)$$

where ε_{W} is the electrolyte dielectric permittivity, n_0 is the ionic charge concentration, N_A is Avogadro constant (1/mol), and i_0 is the ionic molar concentration of the solution.

In this way, the solid–liquid interface is modeled in (2) by a nonlinear voltage source (Ψ_0), which is dependent on pH, ionic concentration, the density of the surface ionizable sites, and their respective dissociation constants [16]. We combine such a dependent voltage source with an established compact model for 2DFETs [11]. In this regard, at the 2-D semiconductor region, the main variables governing the carrier statistics, which are thoroughly explained in [11], are summarized as follows: 1) the quasi-Fermi level ($-qV$), which must fulfill $V(x = L) = V_{\text{d}}$ ($V(x = 0) = V_{\text{s}}$) at the drain (source) edge, where L is the gate length and V_{d} (V_{s}) is the drain (source) voltage, and 2) its shift with respect to the conduction (valence) band edge in an n-type (p-type) ISFET (qV_c). The source/drain electrodes are considered to be passivated so that ions cannot be adsorbed by these metals. In addition, our model considers a trapped charge density in the semiconductor, Q_{it}, computed as [11], [17] $Q_{\text{it}} = qN_{\text{it}}/(1 + \exp((V_c - V_{\text{it}})/V_{\text{th}}))$, where N_{it} is the effective density of trap states and $-qV_{\text{it}}$ is the shift of the effective trap energy level with respect to the conduction/valence band. Then, the trap capacitance C_{it} can be calculated as [11]

$$C_{\text{it}} = \frac{dQ_{\text{it}}}{dV_c} = \frac{qN_{\text{it}}}{2V_{\text{th}}} \frac{1}{1 + \cosh[(V_c - V_{\text{it}})/V_{\text{th}}]}. \quad (5)$$

We can, eventually, find an expression to evaluate the net sheet density assuming a parabolic dispersion relationship and incorporating Fermi–Dirac statistics [11]

$$Q_{\text{net}}(x) = -q^2 D_0 V_{\text{th}} u(V_c); \quad u(V_c) = \ln\left[1 + e^{-V_c/V_{\text{th}}}\right] \quad (6)$$

where $D_0 = g_K(m^K/2\pi\hbar^2) + g_Q(m^Q/2\pi\hbar^2)\exp[-\Delta E_2/k_B T]$ is the 2-D density of states in a two-valley semiconductor, with $\hbar$ the reduced Planck's constant, g_K (g_Q) the degeneracy factor, and m^K (m^Q) the band effective mass at the K (Q) valley. In most of 2-D TMDs, the energy separation between the K and Q valleys, ΔE_2, is only around $2k_B T$ [18], [19] and both valleys participate in the transport process. Further valleys are neglected because they are typically far away in energy to contribute to the electrical conduction under common bias conditions [20]. The quantum capacitance is given by $C_q = dQ_{\text{net}}/dV_c = C_{\text{dq}}(1 - \exp(-u))$ [11], where $C_{\text{dq}} = q^2 D_0$ is the degenerated quantum capacitance, i.e., the maximum value reachable when the 2-D channel is highly degenerated ($V_c \ll -V_{\text{th}}$) [21].

As an explicit expression for V_c as a function of the terminal biases cannot be obtained from (1) and (6), the strategy proposed in [22] and [23] is considered. Basically, it implements a Verilog-A algorithm that iteratively evaluates the chemical potentials at the source and drain edges ($V_{\text{cs}} = V_c|_{V=Vs}$ and $V_{\text{cd}} = V_c|_{V=Vd}$, respectively), allowing the circuit simulator to solve such equations in a moderate run time and, thus, achieving a circuit-compatible model.
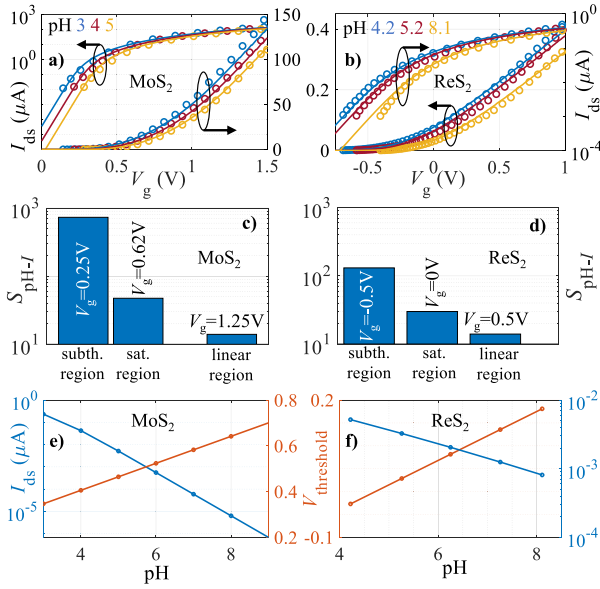
Fig. 2. Transfer characteristics in both logarithmic and linear scales of (a) n-type MoS$_2$-ISFET with 30-nm HfO$_2$ as top oxide and (b) n-type ReS$_2$-ISFET with a top oxide of 20-nm Al$_2$O$_3$; at different pH values. Symbols represent the measurements and solid lines represent the model outcome. The devices are reported in [4] and [5] and described by the parameters collected in Table I. pH current sensitivity in different operation regions for (c) MoS$_2$-ISFET for a change of pH from 4 to 5 and (d) ReS$_2$-ISFET for a pH change from 4.2 to 5.2. Threshold voltage and drain current in the subthreshold region for (e) MoS$_2$-ISFET ($V_g = 0.25$ V, voltage sensitivity of 59 mV/pH) and (f) ReS$_2$-ISFET ($V_g = -0.5$ V, voltage sensitivity of 53.4 mV/pH).
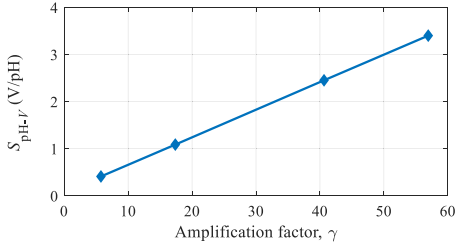

Fig. 3. Voltage sensitivity of the MoS$_2$-ISFET described in Table I, varying the bottom gate bias and setting $V_g = 1$ V for different amplification factors, $\gamma = C_{ox}/C_b$.

Considering a drift-diffusion transport regime, the current of a 2-D-ISFET can be accurately calculated as [11], [24]

$$I_{ds} = \mu \frac{W}{L} C_{dq} V_{th}^2$$
$$\times \left[\left(1 + \frac{C_{dq}}{C_{t,eq} + C_b} \right) \left(\frac{u_s^2 - u_d^2}{2} \right) + \left(e^{-u_d} - e^{-u_s} \right) \right] \quad (7)$$

where $u_s = u(V_{cs})$ and $u_d = u(V_{cd})$, W is the channel width, μ is the electron/hole mobility, and $C_{t,eq}$ is the series combination of C_{eq} and C_{ox}.

The proposed analytical description is implemented in Verilog-A and included in Advanced Design System (ADS).

III. RESULTS AND DISCUSSION: THEORY VERSUS EXPERIMENTS

We have assessed the model against experimental measurements taken from a MoS$_2$-FET pH sensor by Sarkar *et al.* [4] (fabricated on a 270-nm SiO$_2$/Si substrate and with 30 nm of HfO$_2$ as gate dielectric) and a ReS$_2$-ISFET (fabricated on a 20-nm HfO$_2$/Si substrate with a top oxide of 20-nm-thick Al$_2$O$_3$ that passivates the channel) reported by Liao *et al.* [5].

TABLE I
2-D-ISFET MODEL PARAMETERS

	MoS$_2$	ReS$_2$		MoS$_2$	ReS$_2$
	SiO$_2$	Al$_2$O$_3$		SiO$_2$	Al$_2$O$_3$
L (μm)	5	1.72	g_K	2	2
W (μm)	20	3.01	g_Q	6	6
t_{ox} (nm)	30	20	$V_{ds,ext}$ (V)	1	0.1
ε_{ox}	25	9	R_c (kΩ·μm)	1	7.21
t_b (nm)	270	20	μ_0 (cm^2/Vs)	200	6.4
ε_b	3.9	15.4	N_{it} (cm^{-2})	2.5·10^{12}	10^{11}
V_{g0} (V)	0.59	0.175	V_{it} (eV)	0.021	0.07
V_{b0} (V)	0	0	ε_W	80ε_0	80ε_0
m^K/m_0	0.54 [29]	1.53 [30]	pK$_a$	7 [31]	10 [32]
m^Q/m_0	0.58 [29]	1.53 [30]	pK$_b$	7 [31]	6 [32]
ΔE_2 (eV)	0.07 [29]	0.3 [33]	i_0 (mM)	10	10
C_{Stern} (μF/cm^2)	20 [34]	20 [34]	N_s (cm^{-2})	4·10^{14} [31]	8·10^{14} [32]

* R_c represents the metal-2D semiconductor contact resistance, included by connecting lumped resistors to the drain and source terminals [35].

Table I summarizes the model parameters in both cases and the site-binding parameters (N_s, pK$_a$, pK$_b$) of both top oxide–electrolyte interfaces.

Fig. 2(a) and (b) shows our compact model results jointly with the measurements of the transfer characteristics ($I_{ds} - V_g$) of the MoS$_2$- and ReS$_2$-based devices, respectively, at three different pH values (pH = 3, 4, and 5 for [4] and pH = 4.22, 5.26, and 8.11 for [5]) in both logarithmic and linear scales. It must be highlighted the very good agreement achieved in all regimes of operation that evidences the predictive capabilities of the model here proposed. A key figure of merit for pH sensors is the pH current sensitivity, S_{pH-I}, defined as the relative change of the 2-D-ISFET current corresponding to a unit change of the pH value, i.e., $S_{pH-I} = (I_{pH2} - I_{pH1})/I_{pH1} \times 100$, where I_{pH1} and I_{pH2} are the currents at the two different pH values. S_{pH-I} can be readily extracted from our model, as shown in Fig. 2(c) and (d). In the subthreshold region, the drain current has exponential dependence on the gate voltage reaching 731 (131) for the MoS$_2$-(ReS$_2$-)ISFET, while in saturation and linear regions, the relationship becomes quadratic and linear [25], with values of 47 (30) and 14 (14), respectively. These predictions are in excellent agreement to those experimentally achieved: 713 (126), 53 (35), and 13 (14) in [4] (see [5]). In addition, we have employed this model to determine the change of drain current as a function of the pH in the subthreshold region [Fig. 2(e) and (f)]. The pH voltage sensitivity, S_{pH-V} (i.e., the shift of threshold voltage due to pH), is found to be 59 mV/pH (53.4 mV/pH) for the MoS$_2$-(ReS$_2$-) ISFET, which is again in agreement with the measured pH sensitivity in [4] ([5]), a value close to the Nernst limit, showing the extraordinary potential of 2-D-ISFETs for ion detection.

Furthermore, exploiting the model implementation, a double-gate ISFET can be used to increase the threshold voltage shift by taking advantage of the electrostatic coupling between the two gate capacitances [26]. The change in the threshold voltage is in this case modified by the ratio C_{ox}/C_b as follows:

$$\frac{\Delta V_{t,b}}{\Delta pH} = \left(\frac{C_{ox}}{C_b} \right) \frac{\Delta V_{t,g}}{\Delta pH} = \left(\frac{C_{ox}}{C_b} \right) \frac{\Delta \Psi_0}{\Delta pH} \quad (8)$$

where $V_{t,g}$ ($V_{t,b}$) is the top (bottom) gate threshold voltage.

Fig. 3 shows S_{pH-V} for $V_{t,b}$ considering a fixed $V_g = 1$ V, by applying the second-derivative method [27] to the transfer characteristics ($I_{ds} - V_b$) for different pH values of the MoS$_2$-ISFET. As shown in Fig. 3, S_{pH-V} increases linearly with the pH sensitivity amplification factor, $\gamma = C_{ox}/C_b$ reaching values beyond the Nerst limit (~3.4 V/pH). This is consistent with the results achieved by Le *et al.* in [28], who

demonstrated a measured S_{pH-V} of 4.4 V/pH for $\gamma = 33$ for the particular case of monolayer MoS$_2$-based ISFETs.

IV. CONCLUSION

A physics-based compact model for double-gate 2-D semiconductor-based ISFETs has been developed and implemented in Verilog-A. It is therefore compatible with standard commercial circuit simulators. The code is available from the corresponding authors upon reasonable request. The predictive capabilities have been benchmarked against experimental data from two devices based on different TMDs, bringing to light the robustness of the proposed approach to predict the electrochemical behavior of such devices. This model also allows a straightforward application to different 2-D materials and represents a valuable contribution to speed up the design and testing of applications aiming at the detection of analytes in chemical and biological experiments.

REFERENCES

[1] C. W. Lee, J. M. Suh, and H. W. Jang, "Chemical sensors based on two-dimensional (2D) materials for selective detection of ions and molecules in liquid," *Frontiers Chem.*, vol. 7, p. 708, Nov. 2019, doi: 10.3389/fchem.2019.00708.

[2] C. Choi, Y. Lee, K. W. Cho, J. H. Koo, and D.-H. Kim, "Wearable and implantable soft bioelectronics using two-dimensional materials," *Accounts Chem. Res.*, vol. 52, no. 1, pp. 73–81, Jan. 2019, doi: 10.1021/acs.accounts.8b00491.

[3] D.-W. Lee *et al.*, "Field-effect transistor with a chemically synthesized MoS$_2$ sensing channel for label-free and highly sensitive electrical detection of DNA hybridization," *Nano Res.*, vol. 8, no. 7, pp. 2340–2350, Jul. 2015, doi: 10.1007/s12274-015-0744-8.

[4] D. Sarkar, W. Liu, X. Xie, A. C. Anselmo, S. Mitragotri, and K. Banerjee, "MoS$_2$ field-effect transistor for next-generation label-free biosensors," *ACS Nano*, vol. 8, no. 4, pp. 3992–4003, Apr. 2014, doi: 10.1021/nn5009148.

[5] W. Liao, W. Wei, Y. Tong, W. K. Chim, and C. Zhu, "Low-frequency noise in layered ReS$_2$ field effect transistors on HfO$_2$ and its application for pH sensing," *ACS Appl. Mater. Interfaces*, vol. 10, no. 8, pp. 7248–7255, Feb. 2018, doi: 10.1021/acsami.8b00193.

[6] H. Park *et al.*, "Label-free and recalibrated multilayer MoS$_2$ biosensor for point-of-care diagnostics," *ACS Appl. Mater. Interfaces*, vol. 9, no. 50, pp. 43490–43497, Dec. 2017, doi: 10.1021/acsami.7b14479.

[7] A. Toral-Lopez *et al.*, "Assessment of three electrolyte–molecule electrostatic interaction models for 2D material based BioFETs," *Nanosc. Adv.*, vol. 1, no. 3, pp. 1077–1085, Mar. 2019, doi: 10.1039/c8na00109j.

[8] H. Wang, P. Zhao, X. Zeng, C. D. Young, and W. Hu, "High-stability pH sensing with a few-layer MoS$_2$ field-effect transistor," *Nanotechnology*, vol. 30, no. 37, Sep. 2019, Art. no. 375203, doi: 10.1088/1361-6528/ab277b.

[9] N. Masurkar, N. K. Thangavel, S. Yurgelevic, S. Varma, G. W. Auner, and L. M. R. Arava, "Reliable and highly sensitive biosensor from suspended MoS$_2$ atomic layer on nano-gap electrodes," *Biosensors Bioelectron.*, vol. 172, Jan. 2021, Art. no. 112724, doi: 10.1016/j.bios.2020.112724.

[10] Y. Yang and W. Gao, "Wearable pH sensing beyond the Nernst limit," *Nature Electron.*, vol. 1, no. 11, pp. 580–581, Nov. 2018, doi: 10.1038/s41928-018-0166-1.

[11] F. Pasadas *et al.*, "Large-signal model of 2DFETs: Compact modeling of terminal charges and intrinsic capacitances," *NPJ 2D Mater. Appl.*, vol. 3, no. 1, pp. 1–7, Dec. 2019, doi: 10.1038/s41699-019-0130-6.

[12] R. Narang, M. Saxena, and M. Gupta, "Analytical model of pH sensing characteristics of junctionless silicon on insulator ISFET," *IEEE Trans. Electron Devices*, vol. 64, no. 4, pp. 1742–1750, Apr. 2017, doi: 10.1109/TED.2017.2668520.

[13] D. Jiménez, "Drift-diffusion model for single layer transition metal dichalcogenide field-effect transistors," *Appl. Phys. Lett.*, vol. 101, no. 24, 2012, Art. no. 243501, doi: 10.1063/1.4770313.

[14] D. E. Yates, S. Levine, and T. W. Healy, "Site-binding model of the electrical double layer at the oxide/water interface," *J. Chem. Soc., Faraday Trans., Phys. Chem. Condens. Phases*, vol. 70, p. 1807, 1974, doi: 10.1039/F19747001807.

[15] K. B. Oldham, "A Gouy–Chapman–Stern model of the double layer at a (metal)/(ionic liquid) interface," *J. Electroanal. Chem.*, vol. 613, no. 2, pp. 131–138, Feb. 2008, doi: 10.1016/j.jelechem.2007.10.017.

[16] P. Dak, W. Seo, B. Jung, and M. A. Alam, "A physics-based (Verilog-A) compact model for DC, quasi-static transient, small-signal, and noise analysis of MOSFET-based pH sensors," *IEEE Trans. Electron Devices*, vol. 64, no. 3, pp. 1285–1293, Mar. 2017, doi: 10.1109/TED.2017.2651905.

[17] S. V. Suryavanshi and E. Pop, "S2DS: Physics-based compact model for circuit simulation of two-dimensional semiconductor devices including non-idealities," *J. Appl. Phys.*, vol. 120, no. 22, pp. 1–10, 2016, doi: 10.1063/1.4971404.

[18] A. Kormányos *et al.*, "k·p theory for two-dimensional transition metal dichalcogenide semiconductors," *2D Mater.*, vol. 2, no. 2, Apr. 2015, Art. no. 022001, doi: 10.1088/2053-1583/2/2/022001.

[19] F. A. Rasmussen and K. S. Thygesen, "Computational 2D materials database: Electronic structure of transition-metal dichalcogenides and oxides," *J. Phys. Chem.*, vol. 119, no. 23, pp. 13169–13183, 2015, doi: 10.1021/acs.jpcc.5b02950.

[20] E. S. Kadantsev and P. Hawrylak, "Electronic structure of a single MoS$_2$ monolayer," *Solid State Commun.*, vol. 152, no. 10, pp. 909–913, May 2012, doi: 10.1016/J.SSC.2012.02.005.

[21] N. Ma and D. Jena, "Carrier statistics and quantum capacitance effects on mobility extraction in two-dimensional crystal semiconductor field-effect transistors," *2D Mater.*, vol. 2, no. 1, Jan. 2015, Art. no. 015003, doi: 10.1088/2053-1583/2/1/015003.

[22] G. M. Landauer, D. Jiménez, and J. L. González, "An accurate and Verilog-A compatible compact model for graphene field-effect transistors," *IEEE Trans. Nanotechnol.*, vol. 13, no. 5, pp. 895–904, Sep. 2014, doi: 10.1109/TNANO.2014.2328782.

[23] J. Deng and H.-S.-P. Wong, "A compact SPICE model for carbon-nanotube field-effect transistors including nonidealities and its application—Part I: Model of the intrinsic channel region," *IEEE Trans. Electron Devices*, vol. 54, no. 12, pp. 3186–3194, Dec. 2007, doi: 10.1109/TED.2007.909030.

[24] E. G. Marin, S. J. Bader, and D. Jena, "A new holistic model of 2-D semiconductor FETs," *IEEE Trans. Electron Devices*, vol. 65, no. 3, pp. 1239–1245, Mar. 2018, doi: 10.1109/TED.2018.2797172.

[25] X. P. Gao, G. Zheng, and C. M. Lieber, "Subthreshold regime has the optimal sensitivity for nanowire FET biosensors," *Nano Lett.*, vol. 10, no. 2, pp. 547–552, Feb. 2010, doi: 10.1021/nl9034219.

[26] M. Spijkman, E. C. P. Smits, J. F. M. Cillessen, F. Biscarini, P. W. M. Blom, and D. M. de Leeuw, "Beyond the nernst-limit with dual-gate ZnO ion-sensitive field-effect transistors," *Appl. Phys. Lett.*, vol. 98, no. 4, pp. 98–101, 2011, doi: 10.1063/1.3546169.

[27] A. Ortiz-Conde, F. J. G. Sánchez, J. J. Liou, A. Cerdeira, M. Estrada, and Y. Yue, "A review of recent MOSFET threshold voltage extraction methods," *Microelectron. Reliab.*, vol. 42, no. 4, pp. 583–596, 2002, doi: 10.1016/S0026-2714(02)00027-6.

[28] S. T. Le *et al.*, "Quantum capacitance-limited MoS$_2$ biosensors enable remote label-free enzyme measurements," *Nanoscale*, vol. 11, no. 33, pp. 15622–15632, Aug. 2019, doi: 10.1039/C9NR03171E.

[29] W. S. Yun, S. W. Han, S. C. Hong, I. G. Kim, and J. D. Lee, "Thickness and strain effects on electronic structures of transition metal dichalcogenides: 2H-MX_2 semiconductors (M = Mo, W; X = S, Se, Te)," *Phys. Rev. B, Condens. Matter*, vol. 85, no. 3, Jan. 2012, Art. no. 033305, doi: 10.1103/PhysRevB.85.033305.

[30] X. Xu *et al.*, "Green and efficient exfoliation of ReS$_2$ and its photoelectric response based on electrophoretic deposited photoelectrodes," *Mater. Des.*, vol. 159, pp. 11–19, Dec. 2018, doi: 10.1016/j.matdes.2018.08.038.

[31] A. Tarasov *et al.*, "Understanding the electrolyte background for biochemical sensing with ion-sensitive field-effect transistors," *ACS Nano*, vol. 6, no. 10, pp. 9291–9298, 2012, doi: 10.1021/nn303795r.

[32] A. Bandiziol, P. Palestri, F. Pittino, D. Esseni, and L. Selmi, "A TCAD-based methodology to model the site-binding charge at ISFET/electrolyte interfaces," *IEEE Trans. Electron Devices*, vol. 62, no. 10, pp. 3379–3386, Oct. 2015, doi: 10.1109/TED.2015.2464251.

[33] S. Tongay *et al.*, "Monolayer behaviour in bulk ReS$_2$ due to electronic and vibrational decoupling," *Nature Commun.*, vol. 5, no. 1, pp. 1–6, May 2014, doi: 10.1038/ncomms4252.

[34] R. E. G. van Hal, J. C. T. Eijkel, and P. Bergveld, "A general model to describe the electrostatic potential at electrolyte oxide interfaces," *Adv. Colloid Interface Sci.*, vol. 69, nos. 1–3, pp. 31–62, 1996, doi: 10.1016/S0001-8686(96)00307-7.

[35] F. Pasadas *et al.*, "Unveiling the impact of the bias-dependent charge neutrality point on graphene based multi-transistor applications," *Nano Exp.*, vol. 2, no. 3, Sep. 2021, Art. no. 036001, doi: 10.1088/2632-959X/abfdd0.